Towards a fundamental understanding of the effects of surface conditions on fatigue resistance for safety-critical AM applications

G-W Zeng[1,2], M C Monu[1], C Lupton[1], B Lin[1], J Tong[1,*]

[1]Mechanical Behaviour of Materials Laboratory, School of Mechanical and Design Engineering, University of Portsmouth, Anglesea Road, Portsmouth PO1 3DJ, UK
[2]Department of Mechanics, School of Science, Wuhan University of Science and Technology, Wuhan 430065, China

Abstract

Fatigue behaviour in High Cycle Fatigue (HCF) regime has been studied in a 17-4 PH steel produced by an Additive Manufacturing (AM) technique, Selective Laser Melting (SLM). The research was prompted by increasing demands of AM techniques for safety-critical engineering applications. One of the main challenges in as-built AM parts is surface roughness, which gives rise to early crack initiation due to stress concentration leading to fatigue failure. This classical problem has been treated empirically in the past, using mainly stress-based approaches. In this work, we studied the cyclic behaviour of materials at the notch root of typical notch sizes in three material types using the finite element analysis with appropriate material models. Two distinct deformation modes are found: Shakedown or ratchetting, dependent on the applied load level. Selected critical surface locations in a specimen produced by SLM were also examined and the results are found to be consistent with those from the idealised notches. The results shed light on the fatigue damage mechanisms in HCF regime, which may be useful in AM material design and life management.

Keywords: Additive Manufacturing; High cycle fatigue; Finite element; notch; ratchetting; shakedown

1. Introduction

There is strong evidence that surface conditions in as-built (AB) specimens have a considerable influence on the fatigue properties of Additive Manufactured (AM) materials [1-5]. AB specimens are known to exhibit dramatic reductions of some 40–50% of fatigue strength compared with those machined or polished [2-6]. The most detrimental effect is attributed to the surface roughness, which cannot be improved by machining post AM, as machining operation exposes large subsurface pores

* Corresponding author: jie.tong@port.ac.uk

[1]. Although post AM processing methods such as HIP or heat treatment may relieve residual stress, improve microstructure or reduce pores in the bulk, such treatments have little impact on improving surface conditions. Surface roughness has now been recognised as one of the major limiting factors in the application of AM technology in fracture-critical components or structures [7,8].

Conventional engineering treatments of the effects of surface roughness on high cycle fatigue (HCF) strength consider the surface as a series of micro-notches. A stress concentration factor, defined as $K_t = \frac{\sigma_t}{\sigma_0}$, where σ_t is the stress at the notch root and σ_0 is the nominal stress, has been used for characterisation purposes. To overcome the difficulties in measuring the actual geometrical parameters needed to calculate the stress concentration factor for notches, Neuber [9] and Arola & Williams [10] proposed simplified analytical solutions to obtain stress concentration factors based on surface roughness parameters. These models assume a periodic and homogeneous surface typically from machining, but not applicable to surfaces produced by AM approaches, where more irregular surface profiles may be obtained associated with specific AM procedures. More recently, Ås et al [11] proposed a new method using automated FE simulation of surface geometries, obtained from white light interferometry, to predict fatigue life of a physical model; whilst Vayssette et al [12] utilised 3D topography measurements to estimate the HCF strength in AM parts. Although the advances in computed tomography have contributed to more realistic physical characterisation of surface conditions of AM parts, the essential approach to fatigue life estimation remains unchanged, i.e. stress parameters, or variants of a stress component, have been used as "fatigue indicators" [12] to describe fatigue lives in HCF regime.

Such approaches have been accepted for the purposes of fatigue life-time management, but they offer little insight into the mechanisms of fatigue damage, from which more physical models might be developed towards informing material design and life management. This has become highly desirable due to the advent of new AM routes which promise to produce net-to-shape parts, to have a greater control of materials properties through processing towards a unified design and analysis process. To achieve the full potential of AM technology for net-shape production of high quality parts, a fundamental understanding of the effects of surface conditions in AB specimens on fatigue properties must be developed, so that insights may be gained towards design and fatigue life management of AM components and structures for safety-critical applications.

The objectives of this study are: i) To investigate the material behaviour of idealised notches under cyclic loading conditions; ii) to identify the cyclic deformation mechanisms in the HCF regime; iii) to examine the cyclic deformation behaviour in selected critical features from the surface profile measurements of AM specimens and iv) to inform design strategies against fatigue damage in AM parts. Surface roughness measurements and HCF experiments as well as tensile testing were performed on 17-4 PH stainless steel specimens produced by selective laser melting (SLM) [13]. Selected idealised notch sizes and critical surface features were studied in the material under applied HCF loading conditions using the finite element approach, and the evolution of cyclic damage and the mode of deformation were monitored. In addition, FE simulations were also carried out on the same notch features in stainless steel 316L [14] and a nickel-based superalloy, RR1000 [15], using elastic-plastic and visco-plastic material models, respectively. These additional exercises aim at removing potential influence of particular material model types on the simulated material behaviour, so that more generic results may be obtained.

2. Methods

2.1 Finite element analysis

- *The FE models*

The FE analyses were conducted using ABAQUS (6.14-1). Due to symmetry, only half of gauge section of the specimen (Fig.1(a)) was modelled. The geometry of the basic FE model, together with the loading and the boundary conditions, is shown in Fig. 1(b), to which selected notch sizes of a semi-circular shape (Fig. 1(c)) were introduced. All nodes at bottom of the model were fixed in the vertical direction, and the node at the left lower corner was also fixed in the horizontal direction to prevent rigid body movement. Axisymmetric boundary condition was applied to the left side of the model due to symmetry around the global y axis. Refined meshes were introduced in the notch and the smallest element size at the notch root was 0.5μm. Cyclic stresses were applied to the top of model to simulate the loads used in the fatigue experiment of 17-4PH steel; and at stress levels between 40 and 80% the yield stresses for SS316L and RR1000. The evolution of the local stresses and strains at the notch root were captured at a nodal point in the notch root (see Fig 1(c)).

In addition, a simplified surface roughness FE model based on a smoothed 2D roughness profile (Fig. 2(a)) was also constructed to evaluate the effects of surface irregularities on the local material constitutive behaviour (Fig. 2(b) and (c)). A representative surface profile (1mm in length) was introduced to the FE model. Mesh refinement was carried out near the edge of the surface, and the minimum mesh size was 0.5μm. Selected critical locations, identified as critical points A, B and C (Fig. 2(c)), were examined in the FE analysis.

- *The materials models*

Three material model types were implemented for the basic notch model to remove potential influence of material model type on the simulated material cyclic behaviour.

Specifically, for 17-4 PH steel [13], a discretised stress-strain relationship was extracted from the engineering stress-strain curve obtained from the monotonic mechanical testing, and presented in Table 1. The simulated results capture the essence of the experimental results, as shown in Fig. 3(a).

In the case of stainless steel 316L (SS316L), an austenitic material with a yield stress of 280 MPa, a standard elastic-plastic model, available in ABAQUS and used in our previous work [14], was used for the analysis. The model considers both kinematic and isotropic hardening in their basic forms, and the model parameters are shown in Table 2.

In the case of RR1000, a CoCr nickel-based superalloy with a yield stress in the range of 900-1000 MPa developed for high temperature applications, a unified viscoplastic constitutive model was adopted. The material parameters were obtained from the mechanical testing data of RR1000 at 650℃; and the viscoplastic model was implemented in ABAQUS via a user-defined material subroutine (UMAT). The experimental and modelling details were presented elsewhere [15].

- *FE procedures*

A four-nodded bilinear plane stress element (CPS4, ABAQUS) was used to mesh the FE models. Convergence studies were carried out, where the mesh sensitivity near the notch root was examined using selected element sizes from 2um to 0.125um. The simulated von Mises stress at notch root for the selected mesh densities are shown in Fig.3 (b). It seems that a mesh size of 0.5 um would suffice in capturing the notch root deformation, and this was adopted in all FE models.

Finite element computations were carried out over selected number of cycles (30-50) to capture the evolution of the material deformation with cycle at the notch root. The results are presented as normal (in the y-direction) stress–strain loops. Five selected notch diameters (20um, 50um, 100um, 200um and 500um) were examined under the selected cyclic loads: either at the load levels used for the fatigue experimental (17-4 PH steel), or at the load levels of 40-80% of the yield stress of the material (SS316L and RR1000). The same procedures were used for the surface roughness FE model.

2.2 Experimental procedures

- *Material and specimen*

Commercial nitrogen gas atomised 17-4 PH stainless steel pre-alloyed powders were used for specimen fabrication in a 3DSystems ProX300® selective laser melting machine. A primarily austenitic microstructure was obtained, with an average grain size about 5μm. Flat dog-bone specimens were built in a horizontal orientation (perpendicular to loading direction), with the dimensions conforming to the ASTM E8 standard (See Figure 1(a)). Full experimental details are presented elsewhere [13].

- *Surface roughness measurement*

Surface roughness was measured using a Mitutoyo SV-C3200 H4 contact-type profilometer. The parameters adopted for the measurement include measuring speed of 2.00 mm/sec and pitch of 0.0010 mm, respectively. Sampling method was by X-axis pitch. The arithmetic mean deviation (Ra) and the average peak-to-valley heights (Rz) values were averaged from fifteen measurements in the perpendicular (X) and parallel directions to the build direction (Z). Raw roughness data were post-

processed by applying a Gaussian filter in order to reduce noise in the 2D roughness profiles. All surface roughness measurements were carried out in accordance with the ISO 4287 standard [16].

- *Mechanical testing*

Uniaxial tensile tests were carried out on the AB specimens according to the ASTM E8/E8M–09 standard. An Instron 8032 universal testing machine with a 100kN load cell was used for monotonic tensile testing, and the specimens were loaded perpendicular to the build direction. An engineering stress-strain curve obtained is presented in Fig. 3(a) as an average of three tests.

The fatigue experiment was carried out under constant amplitude cyclic loading (R=0.1) on an Amsler vibrophore machine (100kN). The loading frequencies were 75±5 Hz and load control errors were estimated to be within 2%. Selected loads were applied till failure, and engineering stress range at failure is presented as a function of the number of cycles between 10^4 and 10^7. Full experimental details are presented in [13].

3. Results

3.1 Experimental results

A typical 2D surface profile from the surface roughness measurement (2.2) is shown in Fig 2(a), from which three critical points (A, B and C) were identified for the FE analysis. The engineering stress-strain curves were obtained from the monotonic tensile testing, from which an average material constitutive behaviour was assumed. Fig. 3(a) shows a typical engineering stress-strain curve, and simulated results from the tabulated experimental data (Table 1) of 17-4 PH stainless steel.

Fatigue behaviour of the material is shown in Fig 4, where fatigue lives between 10^4 and 10^7, typically in the conventional HCF regime, are presented with the nominal stress ranges applied for the AB specimens. Six stress levels were used in the fatigue experiment and they were subsequently utilised in the FE analysis to evaluate the deformation modes for typical notch sizes (2.1) and critical surface features (Fig.2(c)) taken from the roughness measurement (Fig 2a).

3.2 *Cyclic deformation modes*

- 17-4 PH

Stress-strain loops were obtained at the notch root of selected notch sizes from 20μm to 500μm under the nominal stress ranges as those used in the fatigue experiment (Fig 4). Up to 30 cycles were

simulated and the results are shown in Fig. 5. It is immediate clear that there are two distinct modes in the evolution of cyclic deformation: Plastic shakedown and strain ratchetting, as shown in Fig. 5, the details of the cycle-by-cycle stress-strain evolution under the six stress ranges for the largest (500 μm) and smallest (20 μm) notch sizes. It seems that load level dictates the deformation mode, where shakedown is observed at low stress ranges (406MPa and 427MPa), as opposed to strain ratchetting at high stress ranges (524MPa and 576MPa). Tendency for ratchetting seems to be present already in intermedium stress levels (460MPa and 474MPa). Large notch size merely enhanced the trend, particularly in the cases of strain ratchetting. It seems that, below a stress range of 460MPa, shakedown prevails; whilst strain ratchetting becomes predominant above this stress range.

Cyclic deformation evolution is also examined for the three selected "critical" notch features (A, B, C) from the surface roughness measurement of the specimens (Fig. 2(a)). Fig. 6 shows the responses at features A and C under the six applied load levels (Fig. 4). It is clear that the two distinct deformation modes found for the idealised notch types are consistently observed here also, with shakedown at low stress levels and ratchetting at high stress levels. Interestingly, the severity of the surface roughness seems to dictate the deformation evolution, with significantly greater deformation and predominantly ratchetting mode experienced in feature A than that in feature C.

- SS316L & RR1000

To test the generality of the above trend, the cyclic deformation patterns in typical notches were analysed in a model material, stainless steel 316L, using an elastic-plastic material model which considers both isotropic and kinematic hardening [14; Table 2]. A third material, a nickel-based superalloy, RR1000, was also studied using a unified visco-plastic material model [15, Table 3]. Selected loads were applied so that the nominal stresses applied are within 40-80% of the yield stress of the material. These loads were chosen so that the maximum notch root stresses are within a range of 0.8 to 1.2 of the yield stress of the material, comparable to those used in 17-4PH steel. For these two materials, the two modes of cyclic deformation, shakedown and ratchetting, are also present, whilst large notches produce higher level of damage accumulation than that of small notches in the case of ratchetting strain, as shown in Fig. 7. For 17-4PH and SS316L, it seems that shakedown occurs only at low stress levels, i.e. when the notch root stress is no more than 20% of the yield stress

of the material; otherwise strain ratchetting seems to be the predominant deformation mechanism at high stress levels (>1.2 σ_{ys}). For RR1000, strain ratchetting seems to be dominant when the notch root stress is above the yield stress (Fig. 7(c)).

4. Discussion

Conventionally, when cyclic stress levels are relatively low such that fatigue failure occurs between 10^4 and 10^6 or more, High-cycle fatigue (HCF) regime is assumed. In this regime, material deformation is believed to be predominantly elastic, and fatigue life may be described by a Stress-Life, or S-N curve approach. As a recent review [8] illustrated, this is the default method for the evaluation of fatigue strength of AM materials when comparing with materials produced by conventional means. Although convenient for material ranking purposes and informative of the basic fatigue properties, the approach offers no insight into the damage mechanisms for this important regime for applications, where optimised processing/post-processing routes may be tailored to improve fatigue resistance. This is particularly relevant in AM materials, where surface roughness in AB parts often dictates crack initiation hence HCF lives. The HCF behaviour of AB parts is governed by micro-notch features such as local geometrical discontinuities which act as stress concentrators, with high stress gradients in such locations. Conventionally, in HCF regime, notch effects have been treated empirically by using correction factors. The non-linear characteristics of a notch in low cycle fatigue (LCF) have been considered by a strain-life approach [17], where the local stress and local strain are accounted for in the Neuber's rule [9]. Together with a stress-strain relationship, such as given by Ramberg-Osgood equation, the Neuber's rule has been used for life prediction purposes in LCF regime. Although the latter approach is a step further in recognising the role of non-linear material deformation at notches, the evolution of cyclic damage and its impact on fatigue life have not been explored.

In this work, we have discovered two distinct deformation modes: Progressive increase in strains or strain ratchetting; and saturation of stress-strain hysteresis loops or shakedown, in the evolution of plastic deformation at a notch root in the conventional HCF regime. The trend was verified in three material types using appropriate material models for a range of idealised notch sizes, as well as for selected critical notch features found on the surfaces of 17-4PH steel produced by SLM.

The results show, for the first time, that even in the conventional HCF regime, non-linear material behaviour at a notch root is pronounced, and fatigue damage is of two distinct modes which are highly load-dependent.

It is not unexpected that materials at a notch root experience yielding under relatively low global stress ranges (40% - 80% of yield stress). It is somewhat surprising that the evolution of deformation with cycle presents two distinct patterns: Shakedown at low nominal stresses and strain ratchetting at high nominal stresses. Whilst the former quickly establishes symmetrical steady-state stress-strain loops, the latter exhibits significant stress relaxation as the strain increases (Figs 5, 6). This is significant in challenging the current stress-based approaches to HCF, which are clearly inadequate in the characterisation of fatigue damage. The deformation process seems to be controlled by *strain*, not stress. It is plausible that local material separation will eventually occur at a "critical" strain as the strain increases, leading to micro-cracking and eventual fatigue failure. As an illustration, a small crack (5μm) was inserted in the notch root in a typical case (Fig. 5, case $\Delta\sigma$=524MPa), where the strain at the notch root reached the strain at failure (≈20%; Fig. 3(b)). Fig. 8(a) shows the cracked FE model and Fig. 8(b) shows the simulated stress-strain loops with cycle ahead of the crack tip (5μm). Strain ratchetting is evident close to the crack tip, consistent with our previous work on fatigue crack growth [18]. It seems strain ratchetting is likely to be the predominant mechanism in prompting further cracking once a crack appears, leading to final fatigue failure.

The existence of two types of fatigue damage modes was first identified by Kapoor [19], who proposed that if a stress-strain cycle is "closed", i.e. saturation, then failure takes place by low cycle fatigue such that the Coffin-Manson relationship may be used to predict the number of cycles to failure. If, however, the strain cycle is "open", i.e. the material accumulates uni-directionally, or strain ratchetting, failure occurs when the total accumulated plastic strain reaches a critical value, which is comparable with the strain to failure in a monotonic tension test. He believed that low cycle fatigue and ratchetting are independent and competitive mechanisms, so that failure occurs by whichever corresponds to a shorter life. The phenomenon of strain ratchetting occurs in the direction of increasing tensile strains when the plastic deformation during the loading portion is not opposed by an equal amount of yielding in the reverse loading direction [17, 20].

The existence of two deformation modes seem to be independent of material types or notch size (Fig. 7). The predicted ratchetting strain values depend on load level and notch size, consistent in trend with the results found in [21]. It is interesting to note that consistent results are obtained from three different materials with different constitutive characteristics: A simple power-law type stress-strain relationship for 17-4PH steel; an elastic-plastic model considering both kinematic and isotropic hardening for SS316L and a unified viscoplastic model for RR1000, hence the influence of particular material model type on the predicted deformation behaviour may be removed.

Strain ratchetting is usually associated with asymmetric cyclic loading, as in the present cases (R=0.1), when the plastic deformation during a loading portion is thought not opposed by an equal amount of yielding in the opposite loading direction. Fatigue testing of materials is commonly conducted under symmetric loading (R=-1), hence simulations were also carried out using the surface roughness FE model under fully reversed (R=-1) cyclic loading conditions. Fig. 9 shows the evolution of the stress-strain loops at the selected critical points (Fig. 2(c), (d)) under symmetric loading for 17-4PH steel. The trend at R=-1 seems to be very similar to that at R=0.1 (Fig. 6), in that shakedown at low stresses (406MPa and 427MPa), as opposed to strain ratchetting at high stresses (524MPa and 576MPa); whilst tendency for ratchetting is evident in the intermedium stress levels (460MPa and 474MPa). These results suggest that the two distinct deformation modes are not specific to asymmetric loading.

These results are significant in that i) they challenge the current fatigue life prediction methods in HCF regime as inadequate being essentially empirical and stress-based. It seems that even at low stress levels a strain-based approach should be considered; whilst at high stress levels a critical strain approach should be used due to strain ratchetting; ii) they may provide insight into developing more fatigue-resistance AM materials. Although damage modes are dependent of load levels, the effects of notch size on the accumulation of ratchetting strain are also significant (Figs 5-7), particularly at high stress levels, hence improving surface conditions remains an important goal for AM technology development and application for safety-critical components.

5. Conclusions

Two distinct deformation modes are found in HCF regime: Shakedown and strain ratchetting. The former appears to occur at low stress levels; whilst the latter occurs at high stress levels. The trend appears to be independent of loading type (asymmetric vs symmetric) or material types.

Author Contributions:

MCM performed the monotonic tensile testing and surface roughness measurements; CL conducted the fatigue experiment; GWZ carried out the FE analysis with the assistance of BL. JT conceived the idea and formulated the plans for the experiments and the FE simulations. The research was conducted at the University of Portsmouth.

Acknowledgements: GWZ was supported by a Visiting Scholarship from China Scholarship Council (No.201808420331).

References:

[1] Tammas-Williams S, Withers PJ, Todd I, Prangnell PB. The Influence of Porosity on Fatigue Crack Initiation in Additively Manufactured Titanium Components. Sci Rep 2017;7(1):7308. https://doi.org/10.1038/s41598-017-06504-5.

[2] Wycisk E, Solbach A, Siddique S, Herzog D, Walther F, Emmelmann C. Effects of Defects in Laser Additive Manufactured Ti-6Al-4V on Fatigue Properties. Phys Procedia 2014;56:371-8. https://doi.org/10.1016/j.phpro.2014.08.120.

[3] Wycisk E, Emmelmann C, Siddique S, Walther F. High Cycle Fatigue (HCF) Performance of Ti-6Al-4V Alloy Processed by Selective Laser Melting. Adv Mater Res 2013;816–817:134–9. https://doi.org/10.4028/www.scientific.net/amr.816-817.134.

[4] Greitemeier D, Dalle Donne C, Syassen F, Eufinger J, Melz T. Effect of surface roughness on fatigue performance of additive manufactured Ti–6Al–4V. Mater Sci Technol 2016;32(7):629-34. https://doi.org/10.1179/1743284715Y.0000000053.

[5] Gong H, Rafi K, Gu H, Janaki Ram GD, Starr T, Stucker B. Influence of defects on mechanical properties of Ti–6Al–4V components produced by selective laser melting and electron beam melting. Mater Des 2015;86:545-54. https://doi.org/10.1016/j.matdes.2015.07.147.

[6] Mower TM, Long MJ. Mechanical behavior of additive manufactured, powder-bed laser-fused materials. Mater Sci Eng A-Struct 2016;651:198-213. https://doi.org/10.1016/j.msea.2015.10.068.

[7] Gorelik M. Additive manufacturing in the context of structural integrity. Int J Fatigue 2017;94:168-77. https://doi.org/10.1016/j.ijfatigue.2016.07.005.

[8] Yadollahi A, Shamsaei N. Additive manufacturing of fatigue resistant materials: Challenges and opportunities. Int J Fatigue 2017;98:14-31. https://doi.org/10.1016/j.ijfatigue.2017.01.001.

[9] Neuber H. Theory of Stress Concentration for Shear-Strained Prismatical Bodies With Arbitrary Nonlinear Stress-Strain Law. J Appl Mech 1961;28(4):544-50. https://doi.org/10.1115/1.3641780.

[10] Arola D, Williams CL. Estimating the fatigue stress concentration factor of machined surfaces. Int J Fatigue 2002;24(9):923-30. https://doi.org/10.1016/S0142-1123(02)00012-9.

[11] Ås SK, Skallerud B, Tveiten BW. Surface roughness characterization for fatigue life predictions using finite element analysis. Int J Fatigue 2008;30(12):2200-9. https://doi.org/10.1016/j.ijfatigue.2008.05.020.

[12] Vayssette B, Saintier N, Brugger C, El May M, Pessard E. Numerical modelling of surface roughness effect on the fatigue behavior of Ti-6Al-4V obtained by additive manufacturing. Int J Fatigue 2019;123:180-95. https://doi.org/10.1016/j.ijfatigue.2019.02.014.

[13] Monu MC, Giet S, Lupton C, Dotcheva M, Pani M, Tong J. Mechanical Behaviour of Stainless Steel 17-4 PH by Selective Laser Melting, under review.

[14] Tong J, Alshammrei S, Wigger T, Lupton C, Yates JR. Full-field characterization of a fatigue crack: Crack closure revisited. Fatigue Fract Eng Mater Struct 2018;41(10):2130-9. https://doi.org/10.1111/ffe.12769.

[15] Cornet C, Zhao LG, Tong J. A study of cyclic behaviour of a nickel-based superalloy at elevated temperature using a viscoplastic-damage model. Int J Fatigue 2011;33(2):241-9. https://doi.org/10.1016/j.ijfatigue.2010.08.016.

[16] Leach, R K, The measurement of surface texture using stylus instruments. In: Measurement Good Practice Guide. 37, 1st ed. Teddington: National Physical Laboratory;2001.p.1-37.

[17] Suresh S. Fatigue of Materials. 2nd ed. Cambridge: Cambridge University Press;1998. https://doi.org/10.1017/S0001924000064629.

[18] Cornet, C., L.G. Zhao and J. Tong, Ratchetting strain as a damage parameter in controlling crack growth at elevated temperature. Eng Fract Mech,2009;76(16):2538-53. https://doi.org/10.1016/j.engfracmech.2009.09.005.

[19] Kapoor A. A Re-Evaluation of The Life to Rupture of Ductile Metals by Cyclic Plastic Strain. Fatigue Fract Eng Mater Struct 1994;17(2):201-19.https://doi.org/10.1111/j.1460-2695.1994.tb00801.x.

[20] Bree J. Elastic-plastic behaviour of thin tubes subjected to internal pressure and intermittent high-heat fluxes with application to fast-nuclear-reactor fuel elements. J Strain Anal Eng 1967;2(3):226-38. https://doi.org/10.1243/03093247V023226.

[21] Kolasangiani K, Farhangdoost K, Shariati M, Varvani-Farahani A. Ratcheting assessment of notched steel samples subjected to asymmetric loading cycles through coupled kinematic hardening-Neuber rules. Int J Mech Sci, 2018;144:24-32. https://doi.org/10.1016/j.ijmecsci.2018.05.034.

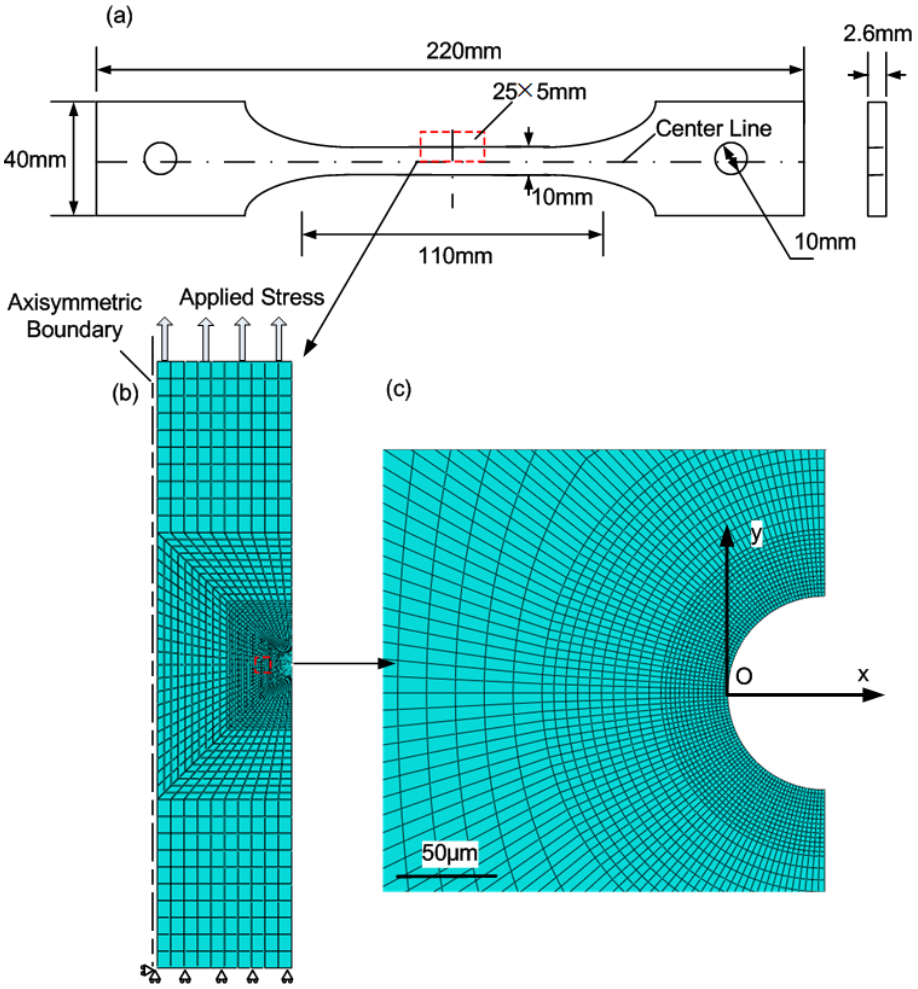

Fig. 1. The specimen and the finite element (FE) model: (a) The dimensions of the specimen; (b) the FE model with the load and the boundary conditions; (c) the refined mesh in the notch root area with a minimum mesh size of 0.5μm.

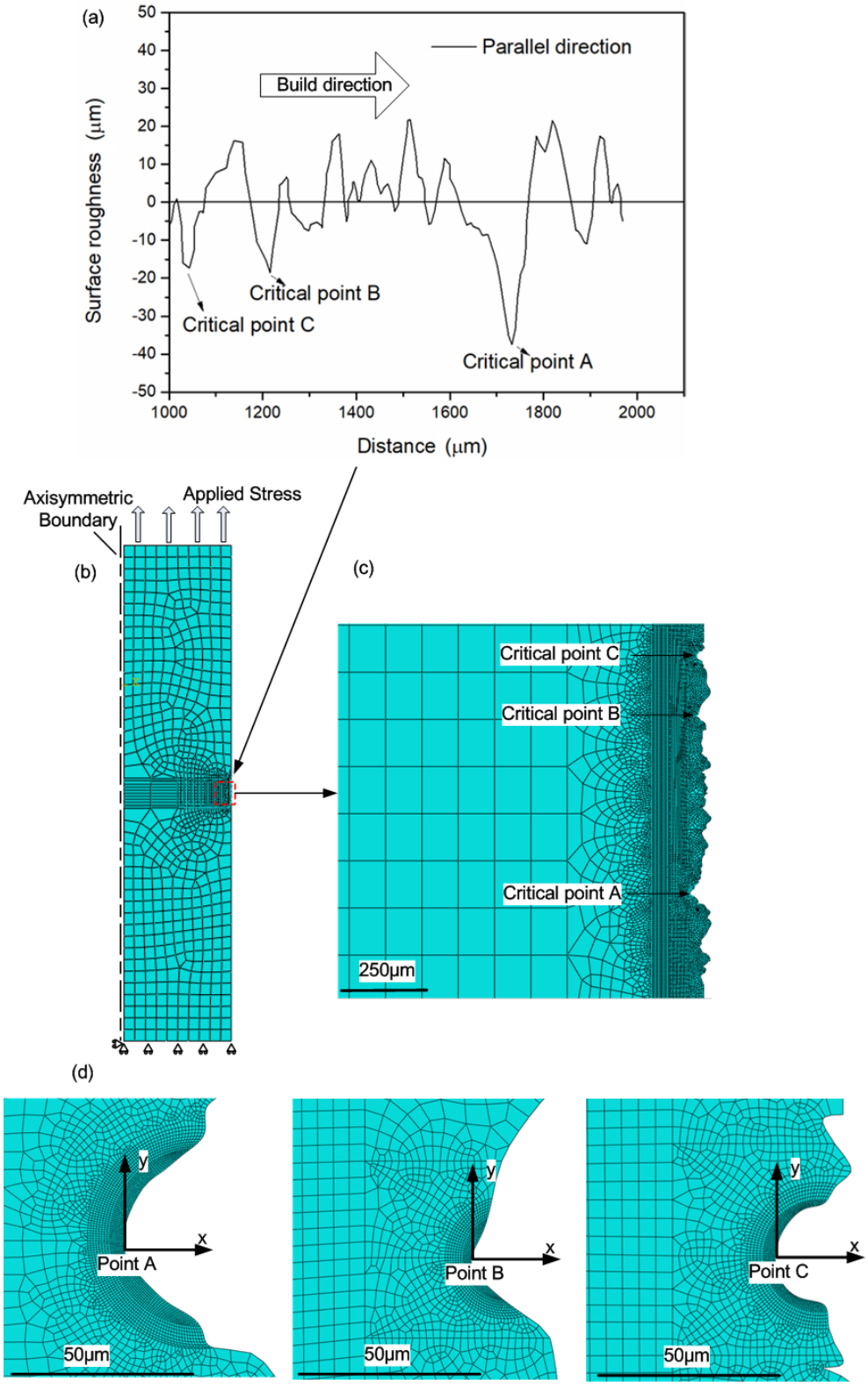

Fig. 2. The surface roughness FE model for half of the tensile specimen: (a) The 2D surface profile obtained from the roughness measurement; (b) the meshed surface roughness FE model after a smoothing procedure; (c) the selected three "critical" points (A, B, C) and refined meshes near these locations; (d) the details of the three critical points, with a minimum mesh size of 0.5μm.

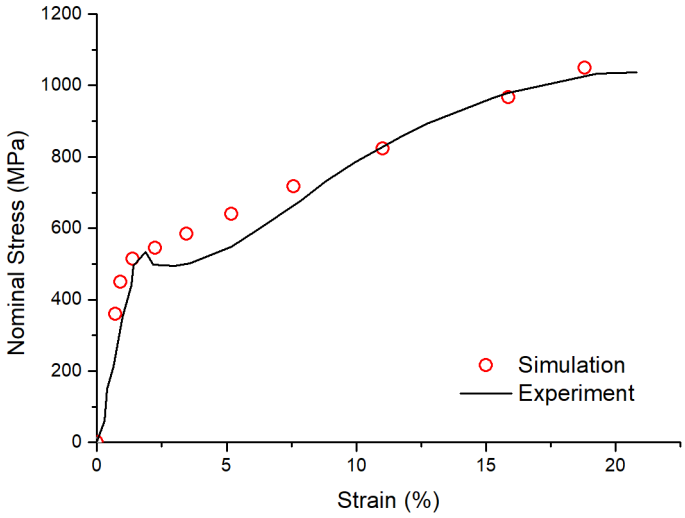

(a)

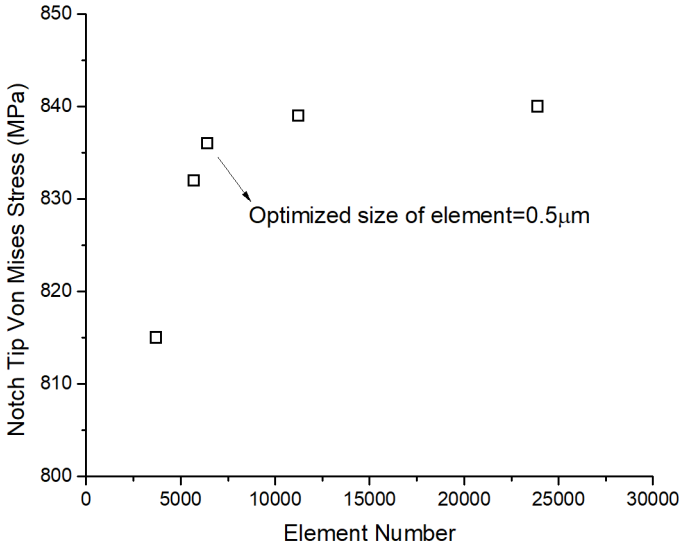

(b)

Fig. 3. (a) The FE simulated and the experimental result of the stress-strain curves of 17-4PH steel, the former was used as the material model in a tabulated format (Table 1); (b) the convergence study, where an element size of 0.5μm was found to be adequate (Notch diameter: 20μm).

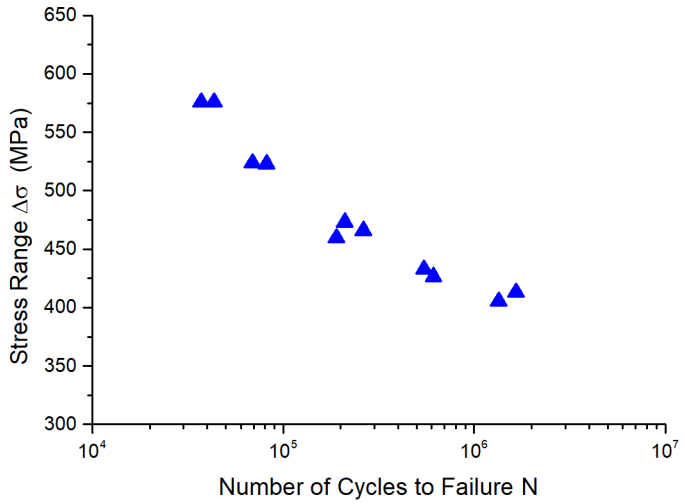

Fig. 4. The S-N curve for the as-built 17-4 PH steel specimens tested under constant amplitude cyclic loading (R=0.1).

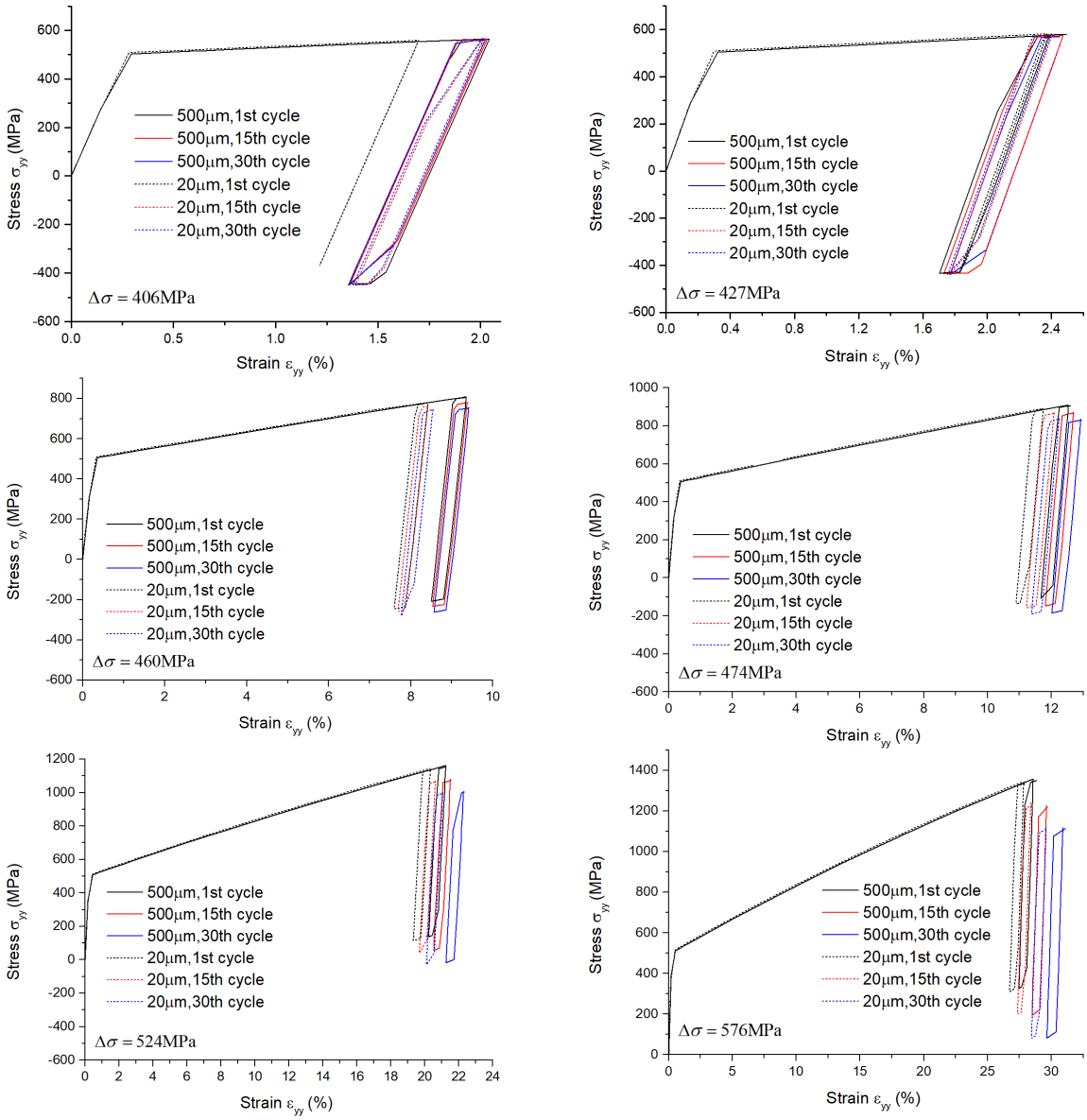

Fig. 5. The evolution of the stress-strain behaviour at the notch root for two notch sizes under the stress levels used for the fatigue experiment (Fig. 4).

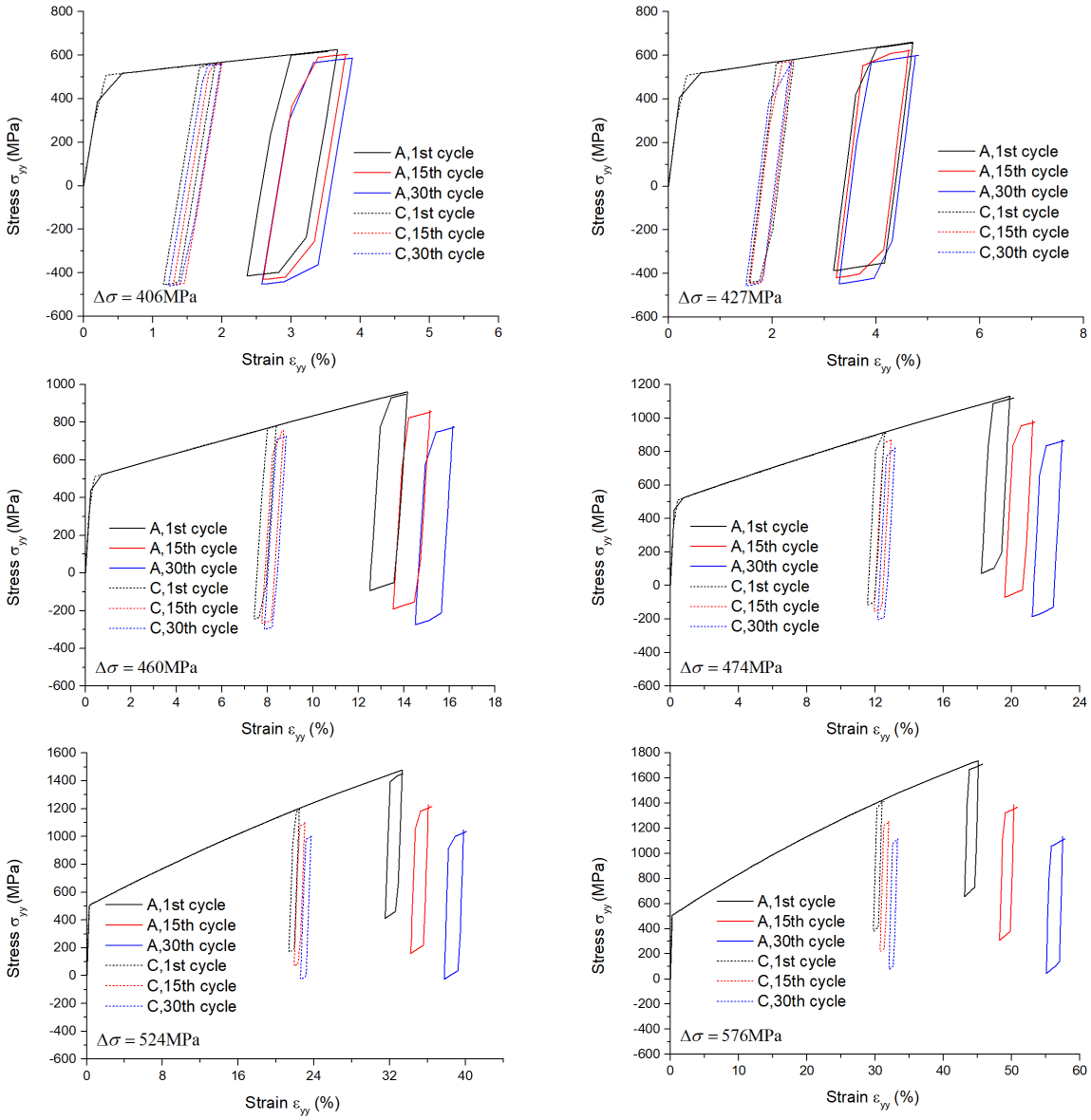

Fig.6. The development of the stress-strain loops at the selected critical points (Fig. 2(c), (d)) with cycle under the loading conditions used for the fatigue experiment (Fig. 4).

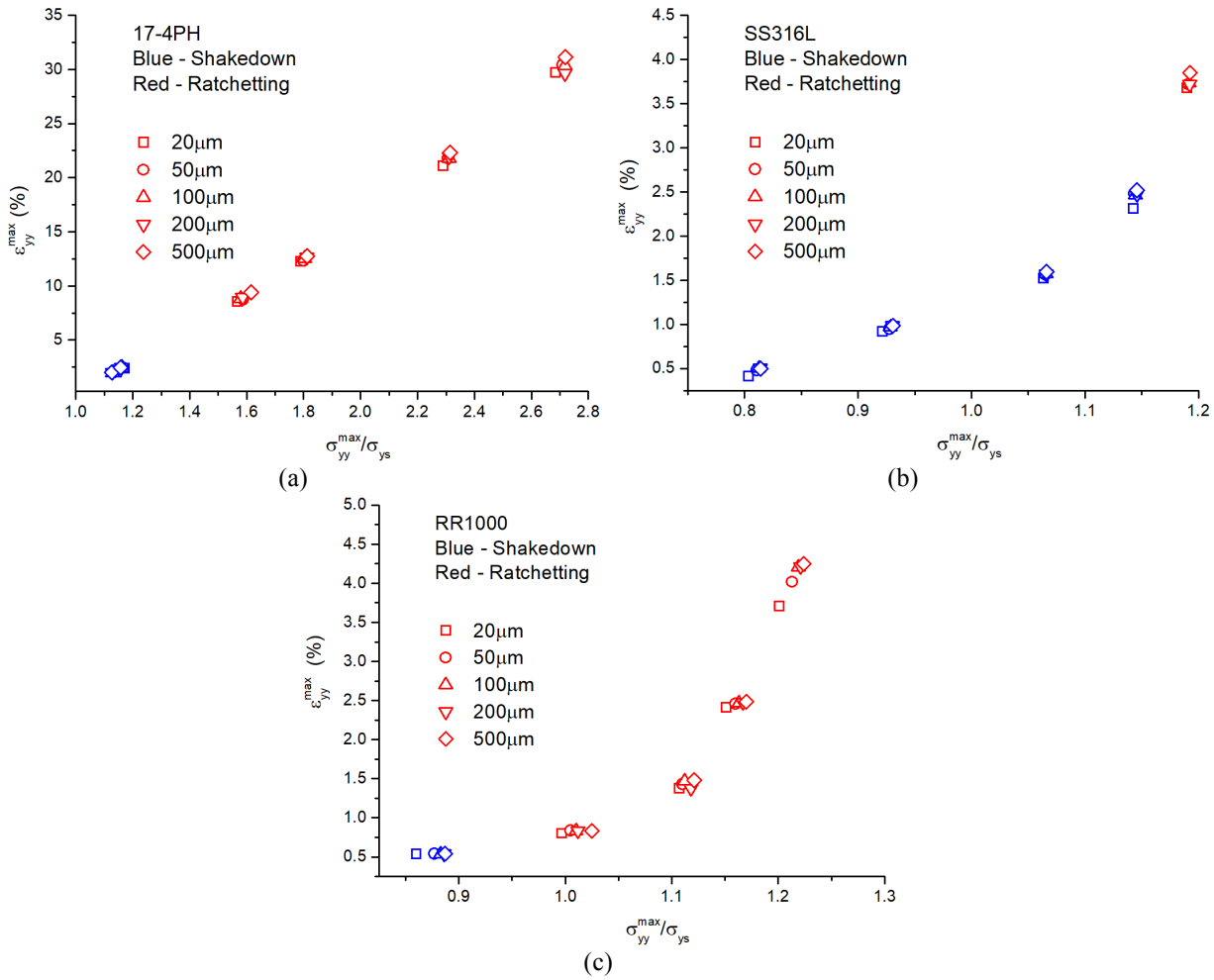

Fig.7. The maximum strains at the end of the simulated fatigue cycles as a function of the normalised notch root stress for the selected notch sizes in (a) 17-4PH steel; (b) SS316L; (c) RR1000.

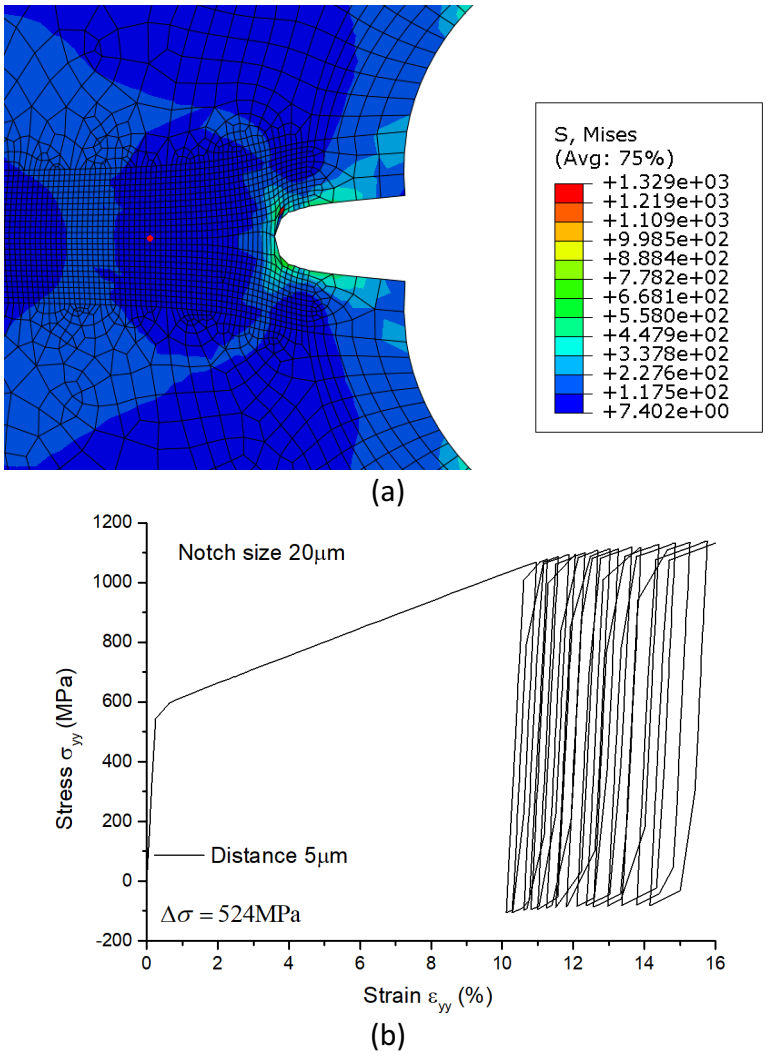

Fig 8. (a) The FE model with a crack (5 μm) inserted in a notch (20 μm; deformed shape); (b) The evolution of the stress-strain loops with cycle at a distance of 5 μm (red dot in (a)) from the crack tip.

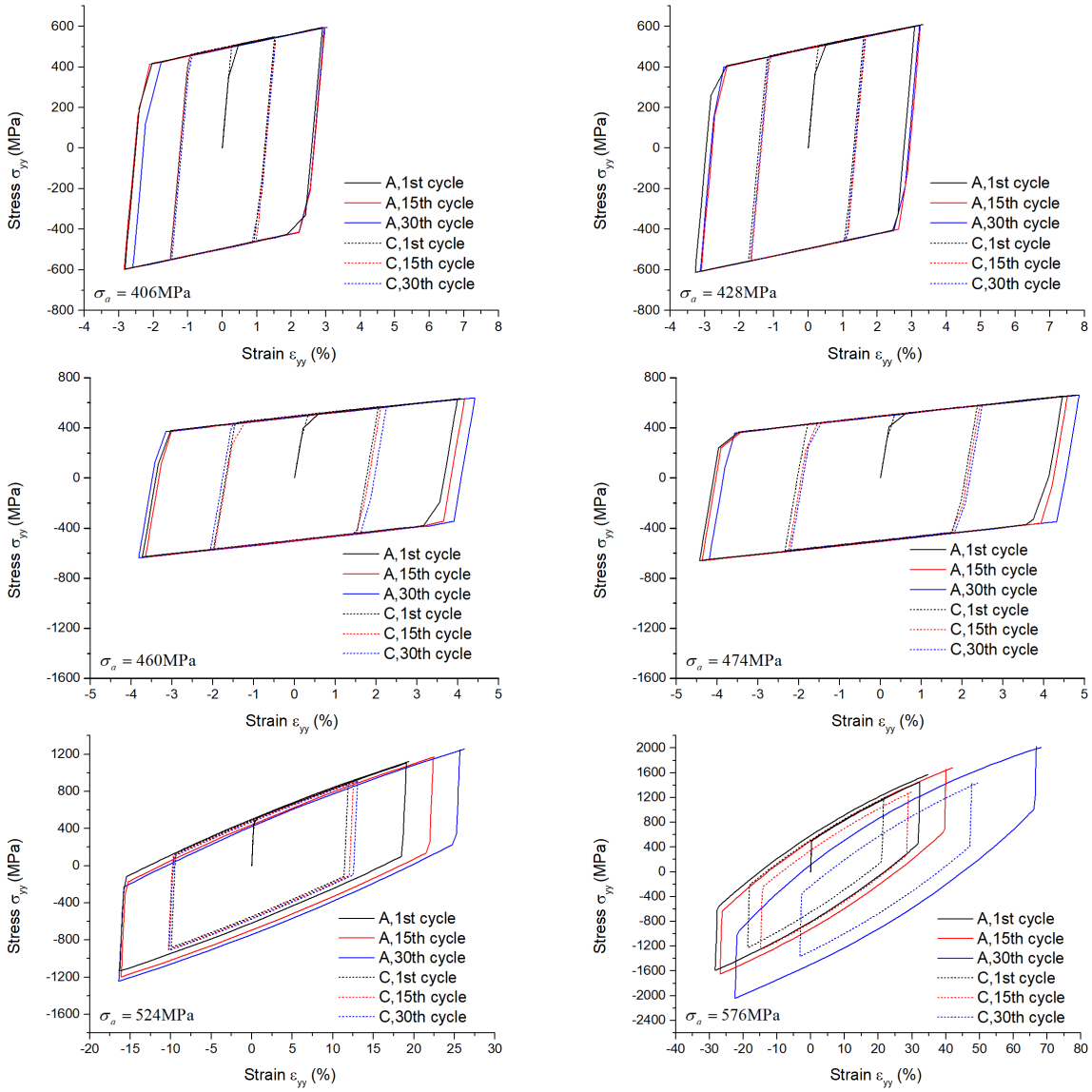

Fig. 9. The evolution of the stress-strain loops at the selected critical points (Fig. 2(c), (d)) under symmetric cyclic loading conditions (R=-1) for 17-4PH steel.

Table 1. The material parameters and model for 17-4PH steel used in the FE analysis.

E(GPa)	ν	Plastic data set	
		Yield stress (MPa)	Plastic strain
190	0.3	502.16	0
		548.97	0.0368
		595.33	0.0453
		676.79	0.0596
		731.25	0.0679
		785.26	0.0778
		859.07	0.0941
		893.73	0.1025
		963.49	0.1252
		979.24	0.1316
		1033.25	0.1641
		1037.30	0.1793

Note: The dimensions of the tensile specimen used in the tensile experiments are: Width = 220.0 mm, height = 40.0 mm and thickness = 2.6 mm.

Table 2. The material parameters for SS316L [14] used in the FE analysis.

E(GPa)	ν	σ_0(MPa)	Kinematic hardening		Isotropic hardening	
			C(MPa)	γ	Q_∞(MPa)	b
193	0.3	100	60000	280	200	6

Table 3. The material parameters for RR1000 [15] used in the FE analysis.

E(GPa)	ν	b	Q(MPa)	a_1(MPa)	C_1	a_2(MPa)	C_2	Z	n	k(MPa)
190	0.285	7.13	161.52	361.57	391.61	266.84	2578.89	678.317	15.496	144.26